

Progress of electrochemical Synthesis of Nitric Acid: Catalyst Design-Mechanistic insights-Protocol-Challenges

Ashadul Adalder, Sourav Paul and Uttam Kumar Ghorai*

Department of Industrial and Applied Chemistry, Swami Vivekananda Research Centre, Ramakrishna Mission Vidyamandira, Belur Math, Howrah-711202, India

***Email:** uttam.indchem@vidyamandira.ac.in; uttamindchem00@gmail.com

Abstract: Nitrogen-based fertilizers are necessary to increase the agricultural output since nitrogen is the most frequent rate-limiting product. The main ingredients in almost all nitrogen-based fertilizers are ammonia and nitric acid; demand for these substances is significantly driven by global population and food production. Over the next few decades, the size and value of the ammonia and nitric acid markets will continue to be largely influenced by global population, which will have a significant impact on energy utility. Ammonia is synthesized via the high energy demanding Haber-Bosch process, and in the Ostwald process, ammonia is catalytically oxidized to prepare industrial grade nitric acid. As industrial synthesis of nitric acid requires astronomical units of energy and emits greenhouse gases into the atmosphere at an alarming rate. Hence, there is an immediate need to find an eco-friendlier alternative route to produce nitric acid. In the approaching century, the most advantageous method that has the potential to significantly alter the human lifestyle is the electrochemical production of nitrate/nitric acid by nitrogen oxidation. In this review article, we have discussed designs of catalysts, mechanistic insights and strategy adapted for in the electrochemical nitrogen oxidation reaction (N₂OR). Emphasis has been made on the various challenges that exist during N₂OR and the possible solution to overcome the hurdles.

Keywords: electrocatalyst, detection protocol, future roadmap, mechanistic insight, nitric acid

1. Introduction: The modernization of agriculture and the use of fossil fuels in the last century have caused a substantial imbalance and redistribution of nitrogen-containing materials. This has prompted interest in developing more resilient and sustainable methods for producing goods that contain nitrogen. Activating an inert chemical bonds and converting them directly into high-value-added products is a good initiative for our society. Dinitrogen, or N_2 , which makes up 78 % of the atmosphere, is easily accessible in nature. But, reactive nitrogen, which is essential for living organisms, is present only in very minute concentrations.[1] The global nitrogen cycle, one of the most significant chemical and biogeochemical cycles on Earth, is built on the conversion of fixed nitrogen into and out of other forms (**Table 1**). Earth has produced fixed nitrogen (150–200 Tg per years) through natural processes for about 2 billion years.[2] About 90% of this can be attributed to the biological fixation of nitrogenase enzymes. A small fraction of Earth's fixed nitrogen comes from air ionization.[3] There have been successes in enacting common chemical bonds, for example, C–H and C–C bonds, [4–5] however initiation of dinitrogen (N_2) with covalent triple bonds is yet lacking for nitrogen fixation. [6–8] Since fixed nitrogen is the most frequent for plant growth, making nitrogen-based compost (nitrate, ammonia, and urea) has been generally challenging worldwide because of its production. For the next thirty years, the use of nitrogen-based fertilizers will only continue to increase global aspirations. [9–10] This will create significant improvement in energy and environment sector because almost all nitrogen-based fertilizers are made using two feedstocks that has high energy and carbon footprint (nitric acid and ammonia). [11] More than half of the world's total fixed nitrogen now comes from anthropogenic sources, including ammonia (100 Tg), leguminous crops (30 Tg), and fossil fuel burning (25 Tg), and these sources are growing. [12–13] Although the

global market for nitric acid (HNO₃) is lower than that of ammonia, it is expanding rapidly because of the development of synthetic fertilizers. The global market value is US \$ 24 billion (market size ~ 70 million tons) with a chemical market value of ~3%. Ammonium nitrate makes up the largest share (80%) in the worldwide nitrate market. [14–16] Ammonia, on the other hand, is largely made industrially using the century–old Haber–Bosch process; one of the greatest discoveries of the early 20th century was that it increased crop productivity by 400%. The Haber-Bosch process has many benefits in feeding the world's growing population, but it has also had some important unintended consequences as it requires ~2% of global energy and emits ~1.5% of greenhouse gases globally. [17–18] Numerous fertilizers and oxidizing reagents contain nitrates or nitric acid. Multi-step methods involving high-temperature, high-pressure conditions are used to produce commercial nitric acid from nitrogen. An alternative method of nitric acid synthesis in an ambient environment is crucial. Commercial HNO₃ was prepared by catalytic oxidation of ammonia (NH₃) using the Ostwald process, followed by multi–step chemical reactions under proper reaction conditions of pressure and temperature are 15–25 MPa and 673–873 K, respectively. [19] These cycles both consume energy–intensive, high global energy and release ozone–depleting substances in worldwide. Due to the effectiveness of non-thermal activation induced by applied potential, electrochemical techniques have been widely utilized in the synthesis of value-added products from nitrogen. The direct nitrogen oxidation reaction, which produces HNO₃ ($2\text{N}_2(\text{g}) + 5\text{O}_2(\text{g}) + 2\text{H}_2\text{O}(\text{l}) = 4\text{HNO}_3(\text{l})$ or $\text{N}_2(\text{g}) + 6\text{H}_2\text{O}(\text{l}) \rightarrow 2\text{NO}_3^-(\text{aq}) + 12\text{H}^+(\text{aq}) + 10\text{e}^-$) by oxidizing nitrogen with oxygen and water, potentially requires significantly less energy than the multistep process. The nitrogen oxidation process requires a Gibbs free energy 87.7 kJ mol⁻¹. [20] The interaction between nitrogen and oxygen is symmetry barred by the molecular orbital mechanism and the N≡N triple bonds in nitrogen molecules are extraordinarily strong (941 kJ mol⁻¹), which makes this process difficult to occur from a

kinetic perspective. [19] Therefore, it is still difficult to identify a suitable catalyst to activate nitrogen molecules and effectively drive the nitrogen oxidation reaction. Electrochemical dinitrogen oxidation process (N₂OR) using various heterogeneous catalysts, such as Ru/TiO₂, Pd-MXene, ZnFexCo_{2-x}O₄, Fe-SnO₂, Nb₂O_{5-x}, Pd-s PNSs, etc., [21–30] under ambient circumstances, are an optimized promising alternative to generate sustainable nitrate products. Processes for electrocatalytic N₂ oxidation proceed in two steps. First, N₂ combines with *O to create an intermediate called NO*, which then undergoes reactions with H₂O and O* to form nitrates, detailed discussion is given in the mechanism portion.

This review is based on outlining the advancements in nitric acid/nitrate synthesis by nitrogen oxidation through an electrochemical route. The history of the nitric acid synthesis process is also concisely presented. A summary of the potential reaction processes is discussed. We compare a set of quantification techniques for measuring the final products after the electrochemical nitrogen oxidation reaction. The role of catalysts and the advantages of different types of electrochemical cells for nitrogen oxidation are also discussed. Finally, the current difficulties and their possible solution for nitrogen oxidation are also covered.

Table 1: Different products produced from nitrogen [20, 29–31]

Reaction	ΔG (eV)	n_e	ΔV (V)	Δe_N
$\text{N}_2(\text{g}) + \text{H}_2\text{O}(\text{l}) + \frac{5}{2}\text{O}_2(\text{g}) \rightarrow 2\text{HNO}_3(\text{g})$	0.93	10	0.093	+5
$\text{N}_2(\text{g}) + \frac{1}{2}\text{O}_2(\text{g}) \rightarrow \text{N}_2\text{O}(\text{g})$	1.07	2	0.535	+1
$\text{N}_2(\text{g}) + 2\text{O}_2(\text{g}) \rightarrow 2\text{NO}_2(\text{g})$	1.08	8	0.135	+4
$\text{N}_2(\text{g}) + \text{H}_2\text{O}(\text{l}) + \frac{3}{2}\text{O}_2(\text{g}) \rightarrow 2\text{HNO}_2(\text{g})$	1.55	6	0.258	+3
$\text{N}_2(\text{g}) + \text{O}_2(\text{g}) \rightarrow 2\text{NO}(\text{g})$	1.81	4	0.453	+2

$\text{N}_2(\text{g}) + 3\text{O}_2(\text{g}) \rightarrow 2\text{NO}_3(\text{g})$	2.46	12	0.205	+6
$\text{N}_2(\text{g}) + \frac{6}{5}\text{H}_2\text{O}(\text{l}) \rightarrow \frac{6}{5}\text{NO}(\text{g}) + \frac{4}{5}\text{NH}_3(\text{g})$	3.90	4	0.975	+2, -3
$\text{N}_2(\text{g}) + \text{H}_2\text{O}(\text{l}) \rightarrow \text{N}_2\text{H}_2(\text{g}) + \frac{1}{2}\text{O}_2(\text{g})$	4.97	2	2.49	-1
$\text{N}_2(\text{g}) + 3\text{H}_2\text{O}(\text{l}) \rightarrow 2\text{NH}_3(\text{g}) + \frac{3}{2}\text{O}_2(\text{g})$	7.03	6	1.17	-3
$\text{N}_2(\text{g}) + 3\text{H}_2\text{O}(\text{l}) \rightarrow 2\text{NH}_2\text{OH}(\text{g}) + \frac{1}{2}\text{O}_2(\text{g})$	7.31	2	3.655	-1
The number of electrons transferred (n_e), voltage per electron (ΔV), and change in nitrogen redox state (Δe_N) are given for free energy change (ΔG , eV) in different reaction.				

2. Roadmap of nitric acid synthesis process

The Birkeland-Eyde method (**Figure 1a**) was one of the most competitive industrial processes for making nitrogen-based fertilizers in the early days. This process requires an electrical arc to react with atmospheric nitrogen and oxygen, eventually adding water to form nitric acid (HNO_3). [32] Birkeland utilized a hydroelectric plant for electricity because the process required about 15 megawatts hour (MWh) per ton of HNO_3 . [33] The reaction step for the formation of nitric acid is given below:

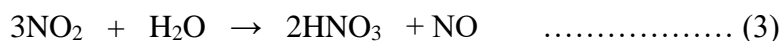


To complete the reaction step 1, it requires high temperature (electric arc/plasma process). Further, hot NO cooled down to normal temperature and combined with O_2 to produced NO_2 .



Reaction step 2 is dependent of the concentration of NO; if the concentration of NO is high then it requires low time for the conversion of nitrogen dioxide. [34]

In step 3, water is used to dissolve NO₂ to form the target product nitric acid.



Overall Birkeland-Eyde process requires high power and energy. The next process in the ninth century came as the Ostwald process (**Figure 1c**) for the formation of nitric acid. In the Ostwald process, oxygen in the air reacts with ammonia (the raw material of the Haber-Bosch process) to form nitric acid in the presence of water. The possible reaction steps are given below: [35]



In the Ostwald process, NH₃ is oxidized at high temperatures (400–600 °C) and high pressure (15–25 MPa) in presence of catalyst to produce nitric acid. This process is highly energy intensive and produces excessive amounts of greenhouse gases (CO₂) in the atmosphere. [36]

Haber–Bosch process (**Figure 1b**) also requires high temperature and pressure (first generation) to form ammonia.[37, 38] Then comes the second generation where the hydrogen evaluation reaction (HER) predominates and the hydrogen produced reacts with nitrogen to form ammonia.[39, 40] But third generation ammonia production where air nitrogen is directly converted to ammonia is using a suitable electrocatalyst catalyst under ambient conditions without applying any temperature and pressure this process is call electrochemical nitrogen reduction reaction (ENRR). [41, 42]

Thus, from an economically sustainable point of view an alternative process would be required which could replace the Birkeland-Eyde process as well as the Ostwald process for

the formation of nitric acid. Recently, researcher fraternity have been working on the direct electrochemical nitrogen oxidation (N₂OR) process that produces nitric acid without applying any temperature or pressure, which will be our future game changer. [18–30, 21, 43] The possible reaction step for N₂OR is given below:

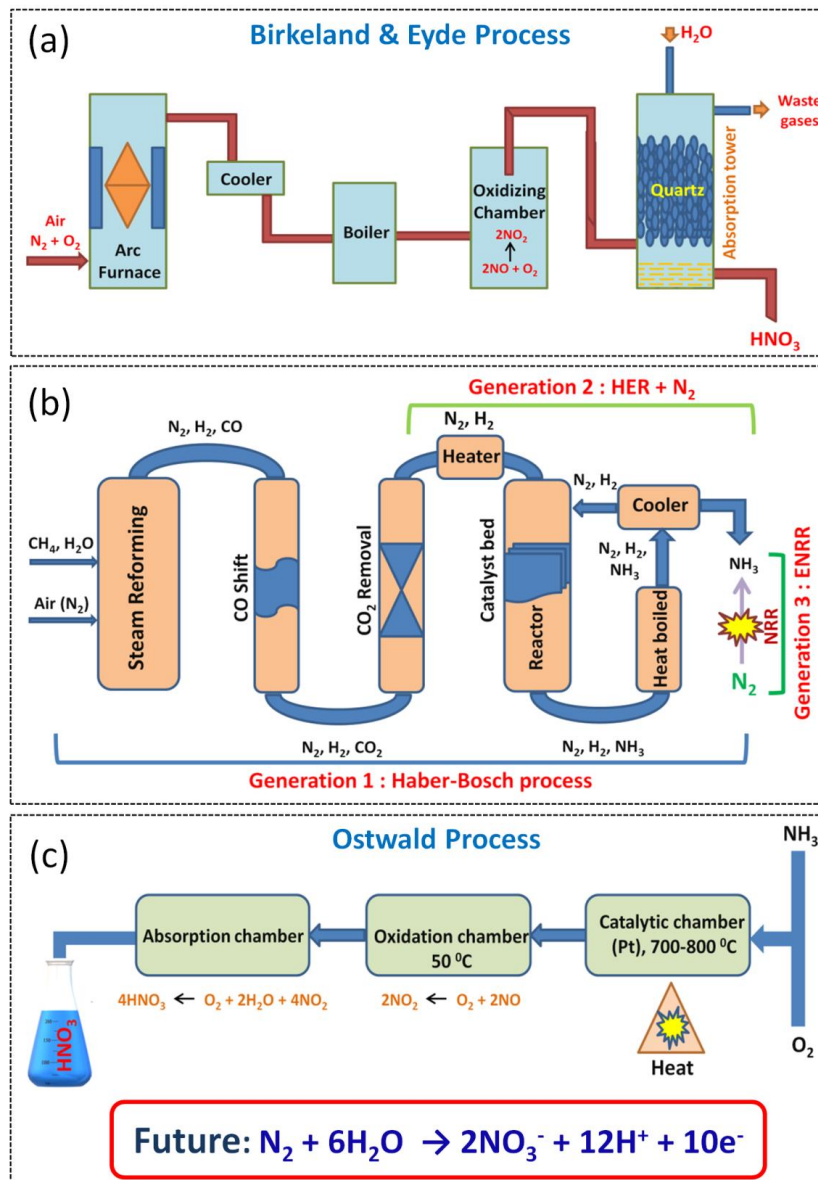


Figure 1: Different types of nitric acid synthesis process, (a) Birkeland & Eyde process (b) Ammonia (raw materials for nitric acid synthesis) synthesis process, (c) Ostwald process

3. Role of electrocatalyst for nitrogen oxidation

3.1 Transition metal based electrocatalyst

Molecular nitrogen (N_2) consists of two nitrogen atoms that covalently bonded with a triple bond $N\equiv N$. This molecular nitrogen is thermodynamically stable and chemically inert as it requires ~ 941 kJ/mol energy to break the $N\equiv N$ to form nitrogen derivatives.[44] Since the initial steps of N_2OR are to break existing $N\equiv N$ bonds and create new $N-O$ bonds, the nitrogen atom does not react easily with oxygen because its $N\equiv N$ bonds are too strong to break. **Figure 2a**, MO of N_2 shows unpaired three electrons (same spin and perpendicular to each other) present in the p-orbital where one p_x is joined (head-to-head) with another p_x to form a sigma (σ) bond in N_2 molecule and other two (p_y & p_z) joins (side by side) other two to form two pi (π) bonds.[45, 46] To break the $N\equiv N$ bond, electrons must jump from Highest Occupied Molecular Orbital (HOMO, σ bonding) to Lowest Unoccupied Molecular Orbital (LUMO, anti-bonding π^*). The energy gap between HOMO to LUMO is very high (10.82 eV) so it is very difficult to break the $N\equiv N$ bond.[44, 47] A variety of transition metals have been used as an electrocatalyst or a cocatalyst to reduce the excess potential required for nitrogen fixation to limit the recombination of charge carriers, and to increase electrocatalytic absorption. Although these advances have resulted in very few systematic studies of the basic processes, they all help to promote higher N_2OR yields. Using a transition metal-based catalyst (present vacant d orbital) can easily break the $N\equiv N$ bond with applied ambient conditions by the synergic effect. During this synergic effect, nitrogen atom shares the bonding σ electrons to vacant d-orbital of the transition metal and accepts the electrons to its π^* anti-bonding orbital by back electron donation from the transition metal (**Figure 2b**).[45, 52] Effectively, this back donation indirectly helps to transfer electrons from HOMO to LUMO which make the $N\equiv N$ bond weaker and easily break to form nitrate.

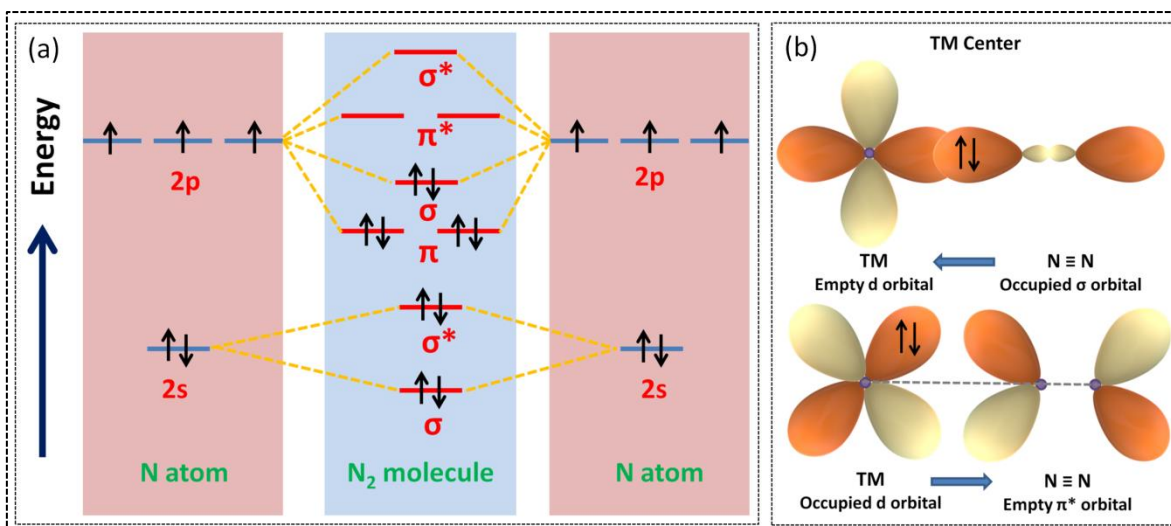


Figure 2: (a) MO of molecular nitrogen; (b) TM role to break the nitrogen bond
[Reproduced from ref. 52]

Bin Zhang et al. [48] used a transition metal; Rhodium (Rh) based nanoparticles (NPs) for electrochemical nitrogen oxidation. Transmission electron microscopy (TEM) image reveals that the average Rh NPs diameter is nearly 5–10 nm shown in **Figure 3a**. Due to the nano structure, it has a more effective surface area for nitrogen absorption which further helps to increase the nitric acid/nitrate production and FE. Initially Rh NPs are inert but in presence of sulfate it shows a good catalytic activity. It is well known that sulfate (SO_4^{2-}) adsorption on the catalyst surface can shift the d-band center of the catalyst to the Fermi level. Rh NPs shows the nitrate production rate nearly $168.0 \mu\text{mol g}_{\text{cat}}^{-1} \text{h}^{-1}$ ($\sim 10.42 \mu\text{g mg}_{\text{cat}}^{-1} \text{h}^{-1}$) and $0 \mu\text{mol g}_{\text{cat}}^{-1} \text{h}^{-1}$ in 0.1 M KOH electrolyte solution with and without 0.5 M SO_4^{2-} , respectively. An atomically dispersed Fe-based catalyst on N-doped carbon nanosheets (AD-Fe NS) (**Figure 3b**) developed by Chunyi Zhi et al.[30] which outperforms as N₂OR catalysts with a record-high nitrate production of $6.12 \mu\text{mol mg}^{-1} \text{h}^{-1}$ (or $2.45 \mu \text{mol cm}^{-2} \text{h}^{-1}$) and Faradaic efficiency (FE) of 35.63%. To activate N₂ and initiate the following N₂OR test, active Fe sites interact with N₂ by hybridizing 3d orbital and N 2p orbital. Haimin Zhang et al. [49] developed an oxygen-coordinated molybdenum (Mo) single atom catalyst bound to carbon (Mo–O–C) using bacterial cellulose (BC) as the carbon source and impregnation

regulator resulting enhancement of N_2OR activities. Bacterial cellulose (BC) is converted to graphitic carbon which resembles a porous structure as shown in TEM observation (**Figure 3c**) and binds with oxygen-coordinated molybdenum (Mo) to form the final structure of Mo–O–C. The Mo–O–C catalyst produces NO_3^- yield rates of $217.1 \pm 13.5 \mu\text{g h}^{-1} \text{mg}_{\text{cat.}}^{-1}$ with a FE of $7.8 \pm 0.5\%$ at +2.35 V vs. RHE.

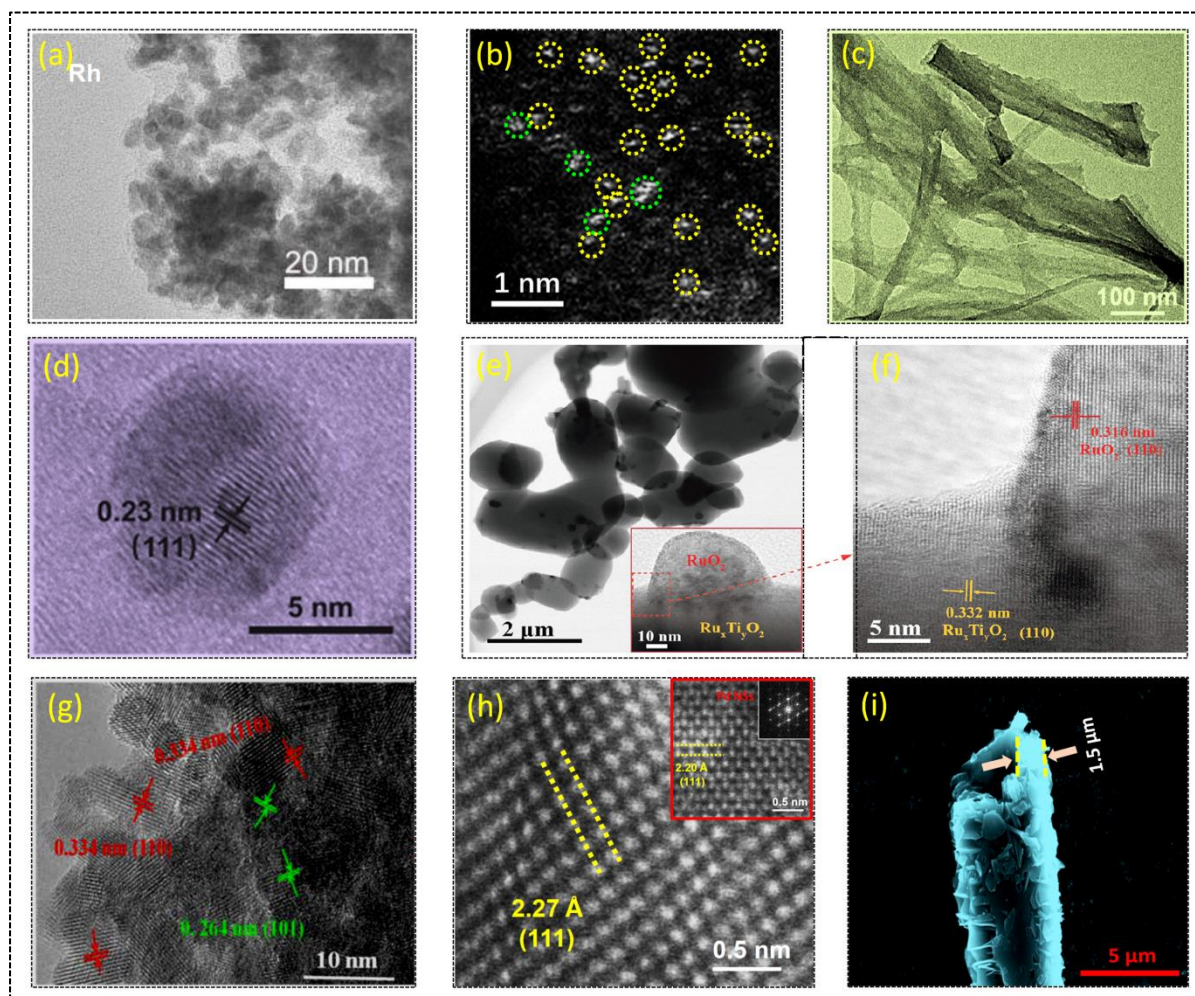


Figure 3. (a) TEM image of Rh NPs. [48] (b) STEM images of AD-Fe NS where single Fe atoms and small Fe clusters are signed by yellow and green dotted cycles, respectively. [30] (c) TEM image of Mo–O–C. [49] (d) HRTEM image of as-prepared Pd-MXene. [27] (e) STEM image and (f) HRTEM image of Ru/TiO₂ catalyst. [28] (g) HR-TEM image of Fe–SnO₂ [23] (h) HAADF-STEM images of Pd-s PNSs [25] (i) SEM image of MnPc HNs [50]

It is widely recognized that nitrogen fixation depends critically on the breaking of strong nitrogen triple bonds. As proof-of-concept electrocatalysts for N_2OR , noble metals (such as

Pd) are used due to the challenge of activating both N_2 and water at relatively low overpotential by taking advantage of their empty d orbital. A common method to maximize the use of noble metals is to use nanometer-sized particles uniformly dispersed on a fixed inert substrate. This creates significant metal active sites that promote enhanced catalytic activity. Qingyu Yan et al.[27] made an electrocatalyst for N_2OR which is evenly dispersed Pd nanoparticles on MXene nanosheet that can produce nitrate in aqueous Na_2SO_4 medium. **Figure 3d** shows a HRTEM image of Pd-MXene where the metallic Pd's (111) plane can be indexed to the lattice spacing of 0.23 nm. At an applied voltage of 2.03V vs. RHE with the Pd-MXene/carbon paper working electrode achieved a NO_3^- yield rate of $2.80 \mu g h^{-1} mg_{cat}^{-1}$ (equal to $45.16 \mu mol h^{-1} g_{cat}^{-1} HNO_3$) with Faradaic efficiency of 11.34%. Qingyu Yan et al.[28] also proposed Ru-doped TiO_2/RuO_2 (also known as Ru/TiO_2) electrocatalyst for N_2OR . Surprisingly, adding Ru to the TiO_2 lattice can cause an upshift in the d-band centre of the Ru site, which increases the Ru site's ability to speed up the electrochemical process that turns inert N_2 into active NO^* . Experimentally, a significant nitrate production rate of $161.9 \mu mol h^{-1} g_{cat}^{-1}$ and the highest Faradaic efficiency of 26.1% are observed for Ru/TiO_2 catalyst in 0.1 M Na_2SO_4 electrolyte medium. **Figure 3e**, STEM supports the growth of RuO_2 nanoparticles on the surface of doped TiO_2 particles, which are about 50 nm in diameter. The reported lattice spacing of 0.332 and 0.316 nm can be assigned to the (110) plane of $Ru_xTi_yO_2$ and RuO_2 , respectively which are slightly larger than the pure TiO_2 (0.322 nm) (HRTEM, **Figure 3f**). In order to obtain highly effective N_2OR catalysts, a new type of Fe– SnO_2 was rationally constructed by Lixue Zhang et al. [23] as a Janus nano electrocatalyst (**Figure 3g**). The yield of NO_3^- was $42.9 \mu g h^{-1} mg_{cat}^{-1}$ and an FE of 0.84 %, this catalyst can also serve as an outstanding N_2OR electrocatalyst. The N_2 adsorption ability is enhanced by oxygen vacancy anchored single-atom Fe, which can efficiently adsorb and activate chemically inactive N_2 molecules and lower the energy barrier for the critical breakdown of nitrogen

triple bond. Tensile strained Pd porous nanosheets (Pd-s PNSs) were fabricated by Bin Zhang et al. [25], and they performed it for electrochemical N₂OR and get the nitrate yield rate of 18.56 $\mu\text{g h}^{-1} \text{mg}_{\text{cat}}^{-1}$ and Faradaic efficiency of 2.5%. According to theoretical calculations, the 3d electron binding energy of Pd can be reduced by adding tensile strain. To verify the authenticity of the claim, scanning transmission electron microscopy was utilized. According to high angle annular dark field scanning transmission electron microscopy (HAADF–STEM) images (**Figure 3h**), Pd-s PNS have a tensile strain increase of ~3.2% $\{(2.27-2.20)/2.20 = 3.18\}$ whereas Pd NS have interplanar spacing of 2.20 Å and 2.27 Å, respectively. Ghorai et al. [50] designed a hierarchical nano–structure (HNs) (**Figure 3i**) of manganese phthalocyanine (MnPc) by solvothermal technique. The presence of HNs absorbed sufficient nitrogen gas which further helped to produce nitric acid after N₂OR under ambient conditions. MnPc–HNs generate nitric acid yield rate of 720 $\mu\text{mol h}^{-1} \text{g}^{-1}_{\text{cat}}$ at 1.9 V vs. RHE and FE of 17.32 % at 1.7 V vs. RHE.

3.2 Non–transition metal based electrocatalyst

The development of an efficient electrocatalyst for the N₂ oxidation reaction (N₂OR) is crucial for achieving green and sustainable N₂ fixation under ambient conditions.[18, 51] Most of the recent studies show that transition metal-based electrocatalysts are the best choice for nitrogen oxidation as previously discussed. There are very few studies based on non-transition metal-based electrocatalysts that can also produce nitrogen derivatives after nitrogen oxidation. A non-transition metal, boron (B) is considered to be a promising catalyst for nitrogen fixation because of its electron deficiency and abundant valence electrons.[52–53] But Boron's data as an electrocatalyst still show limitation for nitrogen fixation due to poor conductivity, weak absorption, and poor activation for nitrogen.[54] It has been found that the inclusion of a second component is an efficient design that can improve the electrocatalytic activity of boron.[54–55] The inclusion of the heteroatom in the core

electrocatalyst can not only modify the band gap of the catalyst but also result in higher charge density and conductivity also helps to reduce the on-set overpotential of the reactants in the electrolysis process by lowering the binding energy.[56–57] It is not technically possible to synthesize a metal-free electrocatalyst using a traditional method because it is very difficult to simultaneously maintain the structure and composition of the material.[58–59] Yongwen Tan and coworkers [29] recently reported a nanoporous boron carbide (np-B₁₃C₂) which can be made by a combination of metallurgical alloy design and chemical etching (**Figure 4a**). The np-B₁₃C₂ shows high catalytic activity and long stability for nitrogen oxidation, which is comparable to the most reported electrocatalysts (comparison in **Table 2**). It can be assumed that the bonds between B and C in np-B₁₃C₂ are mainly sp² hybridization, which leads to higher carrier density and lower resistance, and this indicates that the np-B₁₃C₂ system has a higher electron transfer rate.[60] The positive charge of the boron atom (which comes from charge transfer by carbon) shows a good catalytic center for the making of the B-N bonds and later for the formation of nitrate ions. [61] The np-B₁₃C₂ system has several active sites for nitrogen fixation (**Figure 4b**). The main active sites are the C atom, the B₁ atom (the boron atom attached to the carbon atom), and the B₂ atom (the boron atom away from the carbon atom). The adsorption energy steps of N₂ on the catalysts (ΔE_{N_2}) were calculated (**Figure 4c**) to check the feasibility of nitrogen fixation. The adsorption energies (ΔE_{N_2}) of N₂ on the C atom, B₁ atom, and B₂ atom are -2.001 eV, -2.348 eV, and -3.256 eV, respectively, which shows that B₂ has the most affinity for N₂. It has a strong absorption capacity.

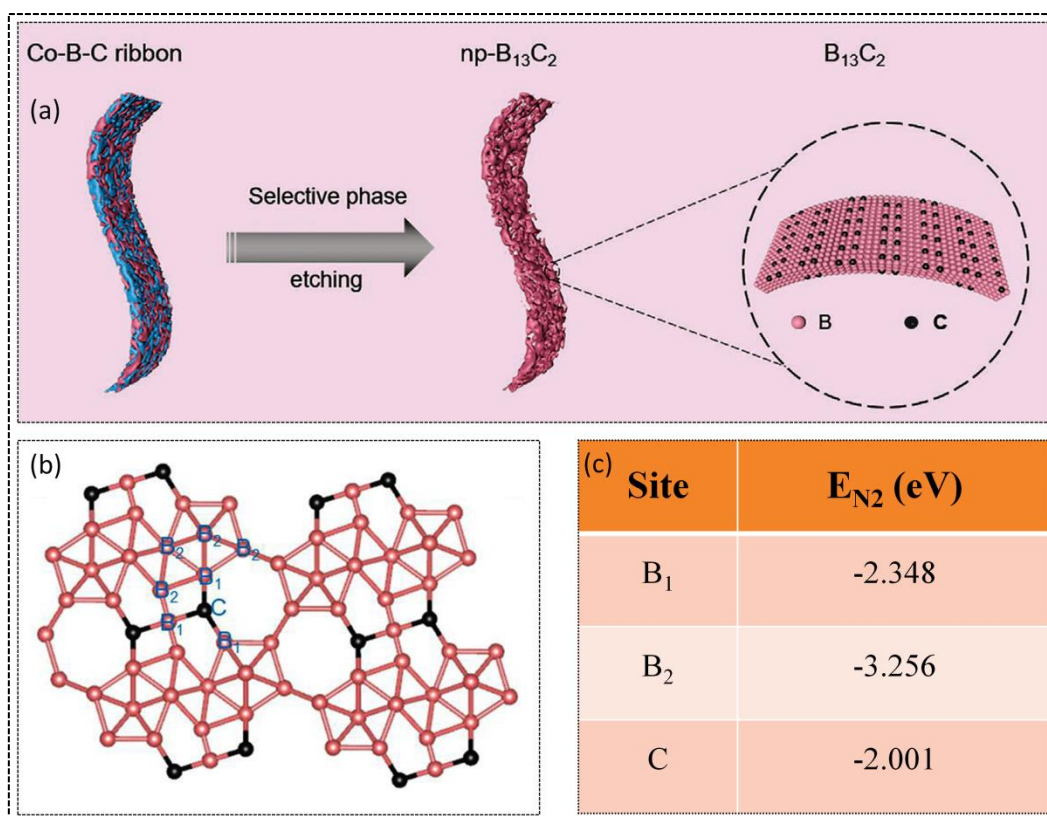


Figure 4: (a) Schematic for fabrication of 3D $np\text{-B}_{13}\text{C}_2$ (b) N_2 adsorption sites on $np\text{-B}_{13}\text{C}_2$ with B_1 , B_2 , C sites (B_1 , boron atom adjacent to the carbon atom; B_2 , boron atom far from the carbon atom). (c) N_2 adsorption energy (E_{N_2}) on B_1 , B_2 , C sites.[29]

4. Mechanistic insights for the formation of nitric acid

Electrochemical molecular nitrogen fixation seems to be a very interesting method for conducting endothermic reactions in ambient conditions, where the required electricity can be provided by the renewable energy sources, thereby making the process sustainable. The equilibrium of the reaction is likely to be 1.32 eV and former reports reveals that the formation of nitrate ions at pH above 1.3 is thermodynamically optimal for the parasitic oxygen evolution reaction (OER).[36] There is a lack of electro-catalysts for the dinitrogen oxidation reaction.[18] At present, several experimental reports have suggested that Pd-decorated MXenes and several oxides have been used as effective electrocatalysts for nitrogen oxidation reactions.[24–28] Presently, Professor Nørskov and his team [62] designed

a theoretical framework for understanding an electrochemical nitrogen oxidation reaction (N₂OR) to nitric acid. They point out several possible rates and selectivity determining primary steps and evaluating the corresponding activation energies.

Considering in **Figure 5a**, a free energy diagram for the bunch of intermediates that feature the easiest path to N₂ oxidation to nitric acid. The free energy for a ten-electron (N₂ (g) + 6H₂O (liq) → 2HNO₃ (aq) + 10H⁺ (aq) + 10e⁻) electrochemical oxidation reaction is in logical protocol with an 11.5 eV experiment when N₂ (g), H₂ (g), and H₂O (g) are utilized as references in standard situations using an SMD (H₂O) / B3LYP-D3 / def2tzvp level of the theory [63]. During oxidation, applying a positive potential may decrease the thermodynamic boundary of N₂OR, but requires an exceptionally high limiting potential of 3.23 V (vs. RHE) for all reactions toward being exogenous. The Vienna Ab initio Simulation Package (VASP)[64–67] with Revised Perdew-Burke-Ernzerhof (RPBE)[68] exchange-interaction functionality is used to provide the best adsorption treatment properties on a solid surface.[69] **Figure 5b** analyzes the gas phase energy of the intermediate response obtained by RPBE utility in VASP and B3LYP-D3 in Gaussian 09. For the current situation, the two functionalities are basically the same as the diagram of the N₂OR cycle. In the section, all electrochemical steps are done on RPBE function. The term entropy has been included in the harmonic approximation for free energy calculations. In the first step (Figure a), it shows that N₂ is adsorbed with OH (coming from water) to form N₂OH which further transform to N₂O (*OH + N₂ → N₂O + H⁺ + e⁻). Also, OH (or *OH) can further oxidize to form O and two O can produce O₂ which is help in oxygen evolution reaction (OER) that reduce the N₂OR process. So choosing a catalyst is important. If a catalyst is good for OER that means it's not so good for N₂OR. When the catalyst is strongly adapted to the N₂OR process, the intermediate N₂O will be converted to HNO₃ by several proton exchange process (N₂O → HON₂O → 2NO → 2HNO₂ → 2NO₂ → 2HNO₃).[62]

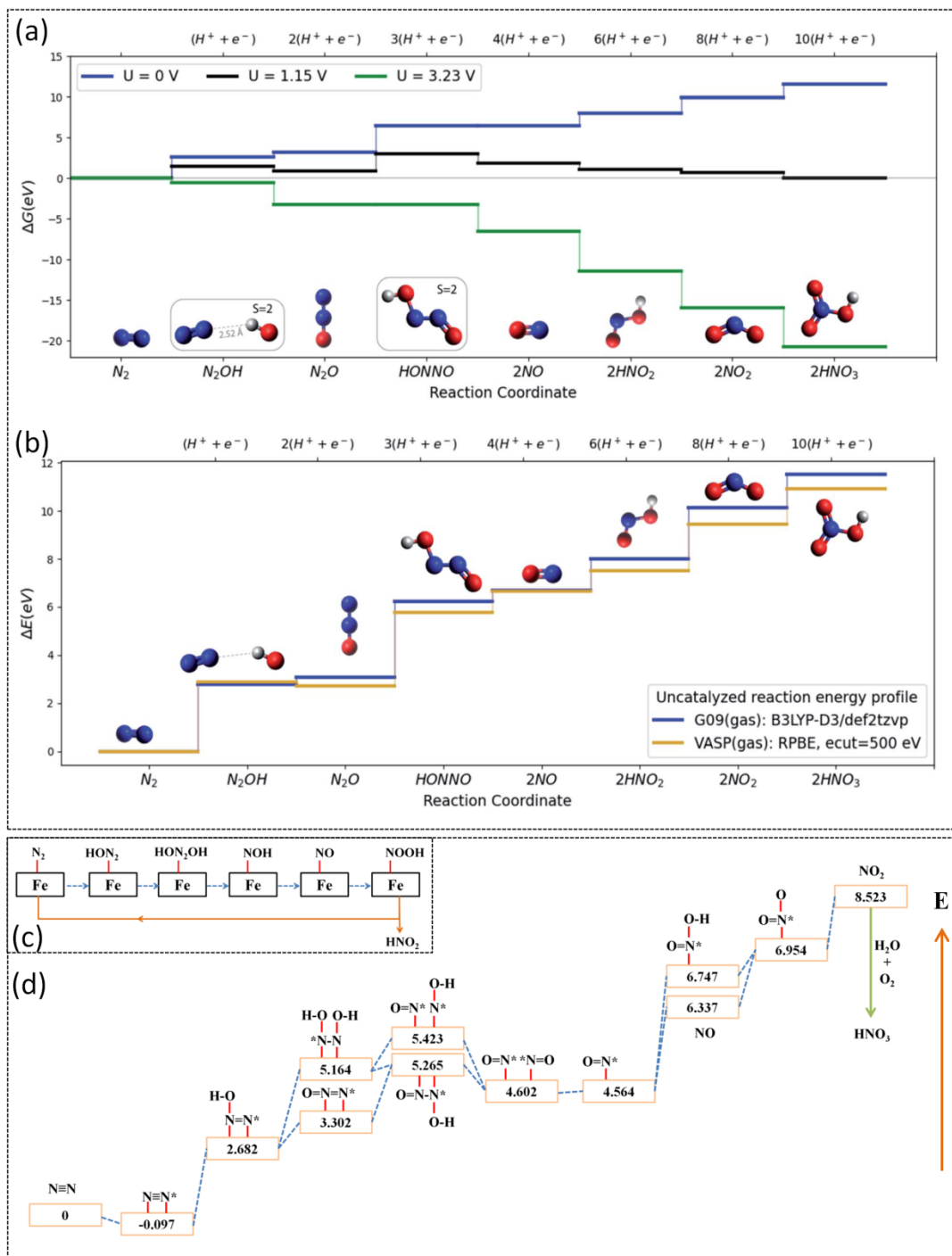
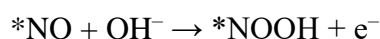
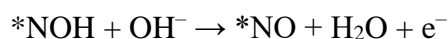
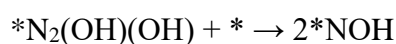
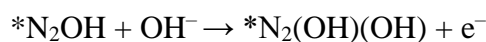
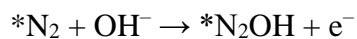
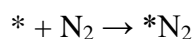


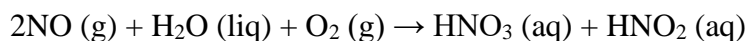
Figure 5 (a) Free energy plot of theory for N₂ to HNO₃ conversion. All the relative free energies (ΔG) are evaluated with respect to N₂ (g), H₂ (g) and H₂O (l). The blue, black and green lines refer to the 0, equilibrium (1.15 V) and the limiting (3.23 V) potentials respectively. (b) Comparison of VASP and G09 energies of the N₂OR reaction intermediates in vacuum.[62] (c) Schematic illustration of N₂OR pathway using AD-Fe NS catalyst [Reproduced from ref. 30] (d) Free energy diagram for N₂ electrooxidation over platinum foil. [Reproduced from ref. 18]

Chunyi Zhi and his coworker [30] have designed a possible N₂OR pathway based on nitrogen oxidation with six primary steps including *N₂, *N₂OH, *N₂(OH)(OH), *NOH, *NO, and *NOOH (**Figure 5c**), in the possibility of oxidation potential. The oxidation reaction of NO₂⁻ + O₂ → NO₃⁻ is a spontaneous reaction and a usual phenomenon in nature, which gives two suggestions: (i) the intermediate *NOOH (namely, NO₂⁻) produced in step 6 easily reacts with O₂ or *OH intermediate and oxidized into NO₃⁻; (ii) when the *NOOH intermediate is released from the catalyst active site and it produces NO₂⁻ in the electrolyte solution where it reacts further with the O₂ (or the O containing oxidative intermediates) and is converted into NO₃⁻. Therefore, the main attention for the electrochemical reaction pathways of the NO₂⁻ production except about non-electrochemical NO₂⁻ to NO₃⁻ reaction step conversion that produces the final product is HNO₂ in aqueous medium.

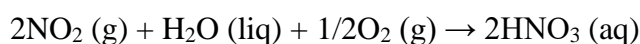


Bin Zhang and his team [18] have synthesis the nitric acid electrochemically by electro-oxidation of nitrogen gas on anode using platinum plate. They also calculated the free energy profile for N₂ electrooxidation to nitric acid on platinum foil using DFT computation. During electrooxidation with continuous nitrogen gas purging into the electrolyte solution, the first, nitrogen molecule was absorbed chemically on the platinum foil surface to form *N₂ with a free energy change of -0.097 eV that indicates the reaction is spontaneous (**Figure 5d**). Then, the active *N₂ reacts with OH⁻ (source water) to form *N₂OH (free energy 2.682 eV). Further, *N₂OH either reacts with another OH⁻ to form *N₂O₂H₂ with a free energy of 5.164

eV or it can be dehydrogenated to *N_2O (3.302 eV). Both *N_2O and *N_2O_2H_2 can produce *NO with an intermediate of *N_2O_2H and *NOH . It is possible *NO could be desorbed from the electrocatalyst surface and react with oxygen in presence of water to form HNO_3 and HNO_2 .



*NO also could react with OH^- to form an intermediate *NO_2H (6.747 eV) which further dehydrogenated to produce an intermediate *NO_2 (6.954 eV). Finally, *NO_2 is desorbed from the electrocatalyst surface to form nitric acid in presence of air and an aqueous medium.



5. Detection protocol of nitric acid/nitrate

There are several methods for detecting nitrate ions (equivalent to nitric acid). One of them is the spectroscopy method (**Figure 6a**). For this procedure, a chemical precursor solution is required before the UV-vis spectrophotometer test. First, 5 ml of electrolyte solution from the oxidation chamber (anodic cell) should be taken in a container and 0.1 ml 1 M HCl should be mixed with the previous solution. The mixture is shaken well for a few minutes and kept for 10 minutes. During the test, a range of wavelengths from 200 nm to 300 nm should be taken. The final spectroscopy absorption value should be taken based on the given equation: $A = A_{220nm} - 2A_{275nm}$. From these absorbance values, the production of nitrate ions is calculated using the prior prepared standard nitrate ions series (MNO_3 ; M is H^+ , NH_4^+ or metal ions) calibration using the above same method. **Figure 6b-c** shows a series calibration of $NaNO_3$ with very accurate R^2 value.[30]

Another detection method, mass spectroscopy can used to verify the nitrate ions generate by the N_2OR experiment using m/z value where m is the mass of ion and z is the charge of ion. If there is produced nitrate ion in the electrolyte solution using $^{14}N_2$ gas then the m/z ($^{14}NO_3^-$):

$m = 14 \times 1 + 16 \times 3 = 62$; $z = 1$) value will be ~ 62 and for $^{15}\text{N}_2$ gas the value will be 63 ($^{15}\text{NO}_3^-$: $m = 15 \times 1 + 16 \times 3 = 63$; $z = 1$). **Figure 6d** shows the MS spectra peak at 61.9899 for $^{14}\text{NO}_3^-$ when $^{14}\text{N}_2$ is purged and 62.9884 for $^{15}\text{NO}_3^-$ when $^{15}\text{N}_2$ is purged. These results show that detected nitrate ions come entirely from electrochemical nitrogen oxidation. [23]

Ion chromatography is a technique where different types of ions (anions or cations) can be detected in solution at ppm or ppb level. IC detector can detect the conductivity ($\mu\text{S cm}^{-1}$) of the ions that present in the solution in Y-axis and in X-axis there has a retention time parameter which is not constant for nitrate ions it may vary by instrument to instrument and eluent flow rate. A standard ions calibration is required to confirm and calculate the concentration of ions present in the solution. A straight line can be drawn from the standard calibration by plotting different concentration (ppm or ppb) of ions vs peak area $\{(\mu\text{S cm}^{-1}) \times \text{min}\}$. **Figure 6e-f** is used to detect the nitrate ions after nitrogen oxidation by IC technique. [27, 48]

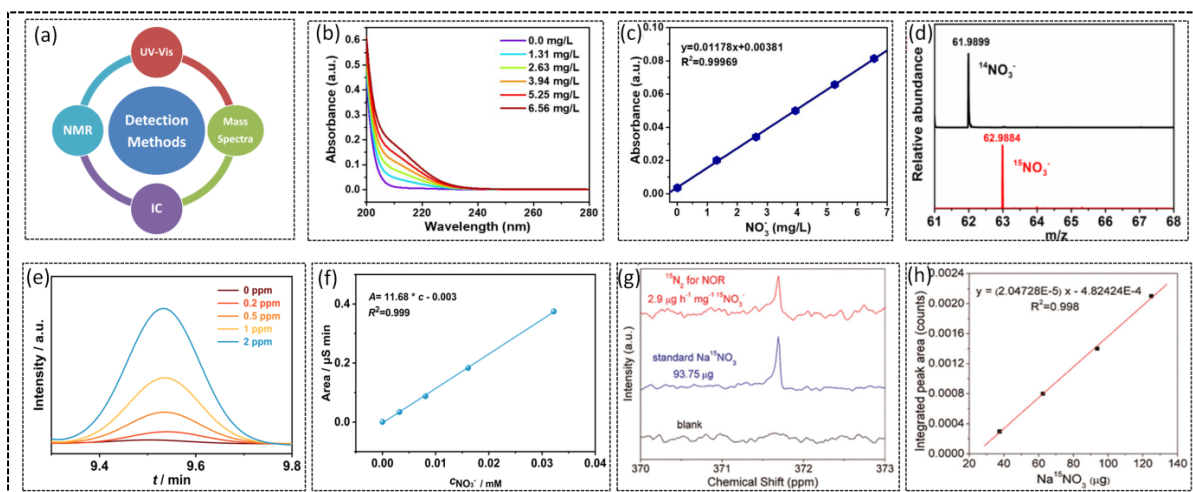


Figure. 6 (a) Schematic of different methods for nitrate ions detection; (b) & (c) UV-Vis curves and calibration curve of standard solution with given NO_3^- concentrations; [30] (d) MS spectra of both $^{14}\text{NO}_3^-$ and $^{15}\text{NO}_3^-$ produced from the N_2OR tests using $^{14}\text{N}_2$ or $^{15}\text{N}_2$ as N_2 source; [23] (e) The quantification of nitrate by IC; (f) IC spectra of the standard nitrate electrolyte with different concentrations (the mass of nitrate in ppm); [48] (g) ^{15}N -NMR spectra (400 MHz) for standard samples of $^{15}\text{NO}_3^-$, blank and the test electrolyte produced from N_2OR using $^{15}\text{N}_2$ feeding gas. (h) ^{15}N -NMR calibration for standard $\text{Na}^{15}\text{NO}_3$. [27]

A piece of natural evidence that the produced nitrate ions are obtained from N_2 feeding is needed to confirm by a $^{15}N_2$ isotope labeling experiment. The typical $^{15}NO_3^-$ signal in the ^{15}N -NMR spectrum may be detected from the electrolyte solution after N_2OR experiments if nitrogen gases are selectively oxidized to nitrate ions. The $^{15}N_2$ isotope (98 atoms% ^{15}N) gases need to be previously purified by passing through a 5% H_2SO_4 solution and a silica gel sorbent tube to remove potential sources of N contamination and then bubbled in the electrolyte solution for half an hour for N_2OR experiments. **Figure 6g** shows an isotopic experiment of N_2OR where the chemical shift value comes at ~ 371.8 ppm range for the sample as well as standard sample. Standard calibration (**Figure 6h**) is made to calculate the concentration of nitrate ions present in the electrolyte solution. [27]

6. Cell design for nitrogen oxidation

It is necessary to strategically design an electrochemical cell as the design can enhance the process by facilitating the mass and charge transfer. Various types of electrochemical cells are reported ranging from single-cell chamber [70] (**Figure 7a**) to dual-cell chamber (H-type cell) [30] (**Figure 7b**) with a three-electrode set-up. In the three-electrode set-up, it comprises of working electrode, reference electrode, and counter electrode, where we can measure/apply a potential in between the working electrode and reference electrode, and we can get/measure a current in between the working electrode and counter electrode. However, most of the research articles reported about the H-type cell for nitrogen oxidation. In an H-type cell, two cell chambers are separated from each other by a cell membrane (primarily Nafion membrane, proton exchange membrane) where the reference electrode and working electrode are present in the anode chamber (oxidation chamber) and the counter electrode is present in the cathode chamber. But there is no such separation in a single-cell chamber.

The advantages of H-type cells over single-cell chambers are that nitrate / nitric acid is produced while electrochemical nitrogen oxidation cannot get transferred from the anode

chamber to the cathode chamber for H-type cells because the two cell chambers are separated by Nafion membrane, only proton (H^+) can go from one chamber to another. Also, it is possible for single-cell to reduce nitrate / nitric acid (in cathode), but not possible for H-type cell.

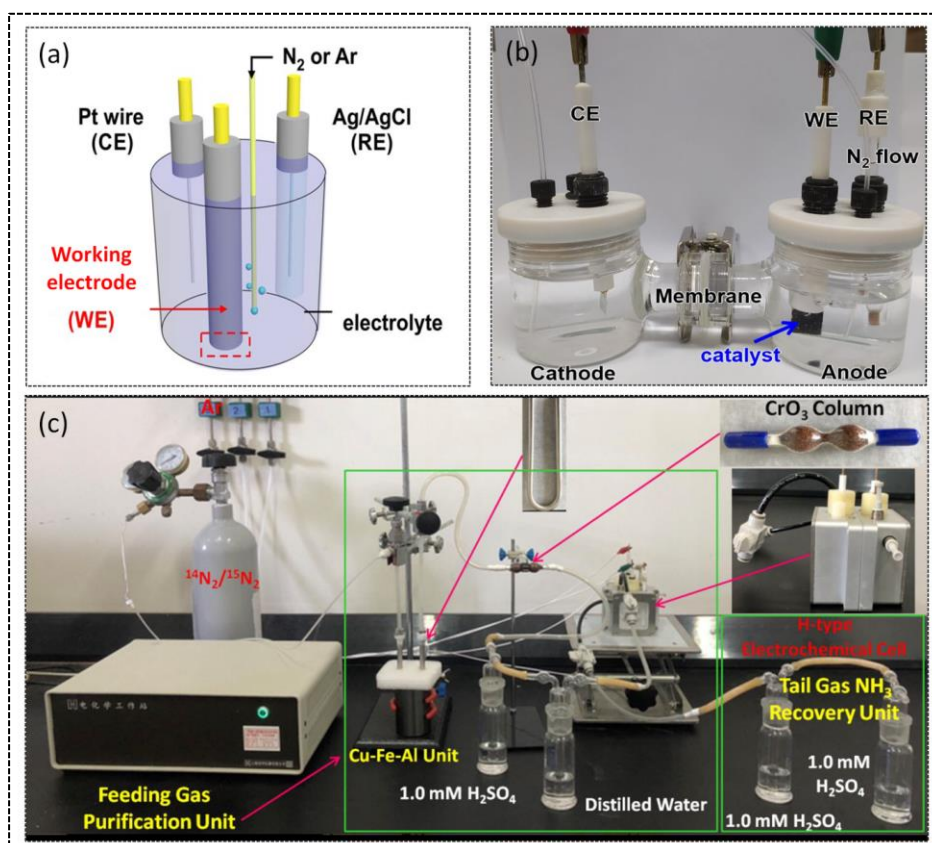


Figure 7: (a) Schematic illustrating of single electrochemical cell for nitrogen fixation,[70] (b) H-type cell setup, [30] (c) Photograph of the electrochemical experimental setup for NRR and N_2OR [49]

Before using the Nafion membrane, it requires a pre-treatment process. The Nafion membrane is pre-treated first in H_2O_2 (5 wt %) aqueous solution for 1 h at 80 °C and then at 80 °C for the next 1 h in ultra-pure water. Prior to the oxidation test, all gases are pre-purified by removing any sources of N contaminant with an basic trap with 0.1 M NaOH, an acidic trap with 0.05 M H_2SO_4 , and a neutral trap with 0.05 M K_2SO_4 . [30] Haimin Zhang et al. designed a purification set-up for nitrogen fixation using a bi-functional catalyst Mo-(O-

C₂).^[48] To ensure quality, a feeding gas purification system was used and all experiments were performed by the protocol. A Cu-Fe-Al catalytic system was used to remove any NO_x contaminants from the N₂ purged gas (**Figure 7c**). The Cu-Fe-Al catalyst-packed stainless-steel column is located in a stainless-steel container filled with a mixture of ethanol (CH₃CH₂OH) and liquid nitrogen (N₂). To remove any NO contaminants in N₂, a CrO₃ column was included in the gas purification set-up to change NO by passing through the Cu-Fe-Al catalytic system to water to form NO₂, which can be eliminated further by H₂SO₄ and distilled water unit before going to the electrochemical cell.

7. Calculation and formulas

After nitrogen oxidation to nitrate or nitric acid production, various results can be calculated by the following equations:

$$\text{Yield rate} = \frac{(C_p \times V)}{(m_{\text{cat}} \times t \times M_p)} \quad [\text{unit: } \mu\text{mol h}^{-1}\text{mg}_{\text{cat}}^{-1}]$$

$$\text{Yield rate} = \frac{(C_p \times V)}{(m_{\text{cat}} \times t)} \quad [\text{unit: } \mu\text{g h}^{-1}\text{mg}_{\text{cat}}^{-1}]$$

$$\text{Yield rate} = \frac{(C_p \times V)}{(S \times t)} \quad [\text{unit: } \mu\text{g h}^{-1}\text{cm}^{-2}]$$

Where, C_p is the concentration of product produced during electrochemical nitrogen oxidation, V is the volume of electrolyte solution taken for electrolysis, t is the total time duration for oxidation for each potential, m is the mass of catalyst, M_p is the molecular mass of the product, and S is the effective catalyst surface area.

Conversion and selectivity can also calculate by the below equations:

$$\text{Conversion} = \frac{\Delta C_p}{C_0} \times 100\%$$

$$\text{Selectivity} = \frac{C}{\Delta C_p} \times 100\%$$

Where, C_p is the concentration of product, C_0 initial concentration, ΔC_p is the concentration difference before and after electrolysis.

Based on different types of electrons transfer mechanism Faradaic efficiency can be calculated by the equation:

$$\text{FE (\%)} = \frac{(n \times F \times C_p \times V)}{(M_p \times Q)} \times 100\%$$

Where, n (= 2, 5, etc.) is the number of electron which come after the balance of the electrochemical reaction, C_p is the concentration of product produced during oxidation process, V is the volume of electrolyte solution taken for electrolysis, F is the Faradaic constant ($96,485 \text{ C mol}^{-1}$), M_p is the molecular weight of the product, and Q is the net charge passed through the electrode.

Table 2: List of different types of electrocatalyst for nitrogen oxidation reaction

Sl. No.	Catalyst	Electrolyte	Potential (RHE)	Yield	FE (%)	Reference
1	Pd-decorated $\text{Ti}_3\text{C}_2\text{T}_x$, (T = F and O)	0.01 M Na_2SO_4	2.03V	Nitrate yield rate of $2.80 \mu\text{g h}^{-1} \text{mg}_{\text{cat}}^{-1}$ (equivalent to $45.16 \mu\text{mol h}^{-1} \text{mg}_{\text{cat}}^{-1} \text{HNO}_3$)	11.34	Chem. Commun., 2020, 56, 5779–5782
2	Pd-s PNSs	0.1 M KOH	1.75V	NOR yield $18.56 \mu\text{g h}^{-1} \text{mg}_{\text{cat}}^{-1}$	2.5	Angew. Chem. Int. Ed. 2021, 60(9), 4474–4478
3	$\text{ZnFe}_{0.4}\text{Co}_{1.6}\text{O}_4$	1 M KOH	1.6V	$130 \pm 12 \mu\text{mol h}^{-1} \text{g}_{\text{MO}}^{-1}$	5.95 ± 0.77 (1.6V) & 10.1 ± 0.9 (1.5V)	Angew. Chem. Int. Ed. 2020, 59(24), 9418–9422

4	Co ₃ O ₄	0.3 M K ₂ SO ₄	2.19V	0.06 μmol h ⁻¹ cm ⁻²	1.23	National Science Review, 2019, 6(4), 730–738
5	Fe–SnO ₂	0.05 M H ₂ SO ₄	1.96V	NOR yield 42.9 μg h ⁻¹ mg _{cat} ⁻¹	0.84	Angew. Chem. Int. Ed. 2020, 59(27), 10888-10893
6	Mo–(O–C ₂) ₄	0.1 M Na ₂ SO ₄	2.35V	217.1 ± 13.5 μg h ⁻¹ mg _{cat} ⁻¹	7.8 ± 0.5	J. Phys. Chem. C 2022, 126, 2, 965–973
7	Nb ₂ O _{5-x}	0.1 M Na ₂ SO ₄	2.4V	2.29 μg h ⁻¹ cm ⁻² (at 2.4V)	2.06 (2.4V) & 9.8 at 2.2V	J. Mater. Chem. A, 2021,9, 17442–17450
8	np–B ₁₃ C ₂	0.1 M Na ₂ SO ₄	2.4V	165.8 μg h ⁻¹ mg _{cat} ⁻¹	8.4	Small 2021, 17, 2102814.
9	Ru–Doped TiO ₂ /RuO ₂	0.1 M Na ₂ SO ₄	2.2V	161.9 μmol h ⁻¹ mg _{cat} ⁻¹	26.1 at 1.8V	Adv. Mater. 2020, 32, 2002189
10	AD–Fe NS	0.05 M K ₂ SO ₄	2.3V	6.12 μmol mg ⁻¹ h ⁻¹	35.63 at 2.1V	ACS Nano 2022, 16, 3432–3432
11	Pd _{0.9} Ru _{0.1}	0.1M KOH	1.7V	0.078 μmol h ⁻¹ mg _{cat} ⁻¹	0.61	ACS Catal. 2021, 11, 14032

8. Challenges and future prospects

The major key issues and their solutions for future prospects are discussed below.

1. The selection of an electrocatalyst for nitrogen oxidation is very important because the catalyst needs sufficient stability or selectivity to absorb nitrogen and break the triple bond to form nitric acid/nitrate. Recent studies show that few research works have been done based on electrochemical nitrogen oxidation reaction and most of them were taken on transition metal-based electrocatalysts due to their synergistic effect and some boron-based electrocatalysts due to their electron deficiency and abundant valence electrons. Thus, studies investigating an electrocatalyst rather than a transition metal-based electrocatalyst are still lacking. If we think about diagonal relationships (showing similar properties) (**Figure 8**) in a periodic table (<https://sciencenotes.org/periodic-table-black-white-wallpaper>) then silicon-based electrocatalyst would be another good choice for the nitrogen oxidation reaction because boron-base electrocatalyst can do N₂OR. There are some studies on bismuth-based

electrocatalysts that can selectively absorb nitrogen for nitrogen reduction reactions. [71, 72]

Thus, it can also be used as a bismuth-based electrocatalyst for nitrogen oxidation.

Figure 8: Periodic table for better representation of selection of catalyst

2. Another important issue is the selection of the working electrode. All research works uses carbon paper, Ti foam, and Pt plate/foil as working electrodes for the nitrogen oxidation reactions. As nitrogen oxidation reaction, conversion of nitrogen to nitric acid/nitrate requires a specific potential that is quite high. Among the three substrate (carbon paper, Ti foam, and Pt plate/foil), carbon paper has the lowest equilibrium oxidation-reduction potential, so the carbon paper may oxidize and produce CO/CO₂. After long time (more than 10 to 15 h) oxidation process on carbon paper, carbon paper will transfer brittle to flexible (**Figure 9**). Also, some papers show that Pt or Ti-based electrocatalysts help to oxidize nitrogen. [18, 28] Therefore, it is very difficult to select a working electrode that remains passive and has good electron transfer capacity during the nitrogen oxidation reaction at applied oxidation potentials. Among these three, carbon paper is less expensive than Ti-foam and Pt plate/foil

but carbon paper will have a chance of oxidation and results may vary after several experiments. Still, the most popular choice for N_2OR is Ti-foam as a good working electrode.

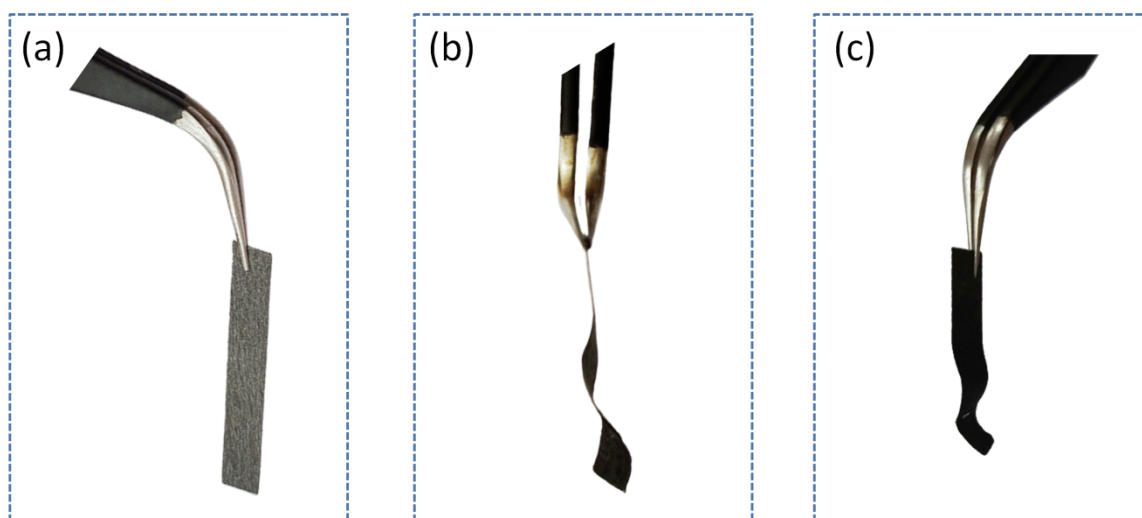


Figure 9: (a) Carbon paper before oxidation (b) & (c) Carbon paper after oxidation

3. Nafion membrane is used in H-type cells for separation between anode and cathode chambers. A polytetrafluoroethylene (PTFE) side chain backbone with ether groups and a sulfonic acid unit at the end make up most Nafion membranes. Before using the electrochemical cell, it should undergo a proper treatment process otherwise the results may vary. Also, since Nafion membrane only passes protons for N_2OR it is really necessary to select the right grade of Nafion membrane. Also be careful of leakage at Nafion junction points.

4. The choice of electrolyte with optimized pH condition is important where the chemical reaction is spontaneous or not. An E–pH diagram sometimes referred to as a Pourbaix diagram, shows the pH and potential values at which a species is thermodynamically stable. Marcel Pourbaix first introduced diagrams in 1938 as a simple way to talk about the chemical properties of species in natural medium (water). Environmental and corrosion science finds diagrams to be particularly helpful. Pourbaix diagrams can be used to predict

the spontaneous direction of electrochemical reactions, identify corrosion products, and predict the changes in environmental potential and pH that lead to higher or lower corrosion attack.[73] A Pourbaix diagram illustrates the potential and pH range over which different species are stable in aqueous medium. The sloping line separates species related by both electron and proton transfer, whereas a horizontal line separates species related by electron transfer only. A vertical line separates species related only by proton transfer. The thermodynamic feasibility of oxidative fixing N_2 (N_2OR) into its oxides is higher than that of a reductive process, particularly under neutral/alkaline conditions (**Figure 10 a**), where the N_2OR is more advantageous than the rival four-electron OER. This suggests that electrochemical N_2 oxidation (N_2OR) into nitrate (NO_3^-) is feasible [30, 36]. It is to be noted that at $pH > 1.3$, N_2OR is more thermodynamically favorable than OER. [36]

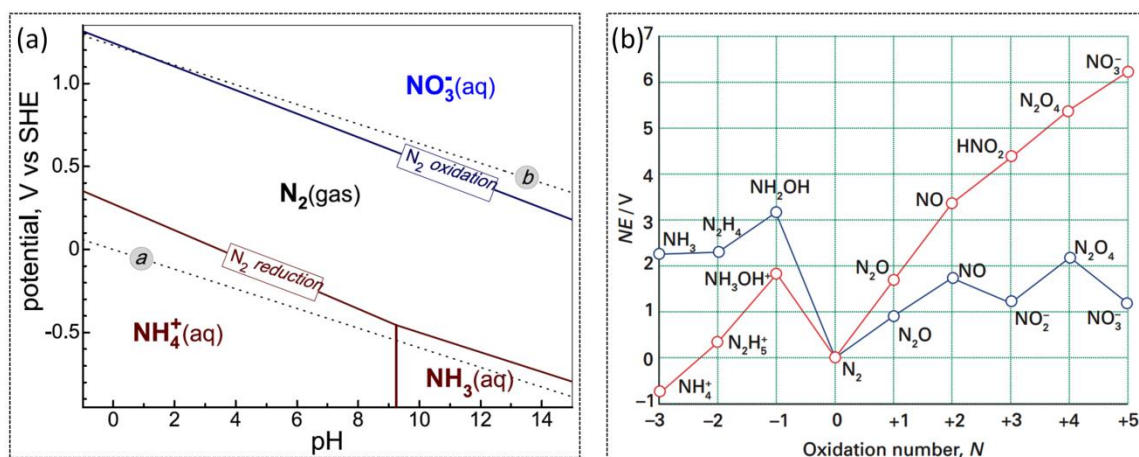


Figure 10: (a) Partial Pourbaix diagram for the N_2 - H_2O system [36] (b) The Frost diagram for nitrogen [74]

The relationship between the Gibbs energy to form different oxidation states of an element and oxidation number is illustrated in a Frost diagram. The lowest-ranking species of an element on the Frost diagram corresponds to its most stable oxidation state. A plot of NE for the pair $X(N)/X(0)$ versus the element's oxidation number, N, forms a Frost diagram

(sometimes referred to as an oxidation state diagram) for an element X (**Figure 8b**) illustrates a Frost diagram in its general form. Frost diagrams show which species $X(N)$ is a good oxidizing or reducing agent depending on the situation. They serve as a useful reference for determining whether the oxidation state of an element is inherently stable or unstable. The standard potential for the couple is higher for the steeper the slope of a line in the nitrogen Frost diagram. Standard (acid) circumstances ($\text{pH} = 0$) are represented by the red line, while $\text{pH} = 14$ is represented by the blue line. Because HNO_3 is a strong acid, it should be noted that even at $\text{pH} = 0$, its conjugate base, NO_3^- , is still present.[74]

5. Isotopic tests are essential to prove the origin of $\text{NO}_3^-/\text{HNO}_3$ formation. This isotopic test should be performed in appropriate conditions for several reasons. First, we cannot purchase 100% pure isotopic gas, it has about 98 to 99.8% (Sigma-Aldrich) pure gas and therefore it needs a proper purification setup before use. Second, the isotopic gas will appear in the cylinder/container under very low pressure, so proper conditions must be maintained before opening the cylinder/container otherwise it may result in loss of the isotopic gas.

6. For nitrogen oxidation, the primary step is the solubility of nitrogen in an electrolyte medium which is further adsorbed on the catalyst surface. Solubility of nitrogen (N_2) at 20°C and 1 bar pressure in water is nearly 20 mg/L. But the solubility of nitrogen gas can increase using an aprotic liquids electrolyte but the mechanism will be complicated. To make more soluble nitrogen gas, we need to purge more nitrogen gas but for absorption of nitrogen gas, it depends on the catalyst surface. If a catalyst absorbed a greater number of nitrogen gas, then it will increase the yield as well as Faradaic efficiency. Choosing a porous catalyst or the presence of a defect side in a catalyst will be a good option for nitrogen absorption where nitrogen can easily absorbed on the porous or defect sides of the catalyst.

7. It is important to pay close attention to the electrochemical N_2OR to $\text{NO}_3^-/\text{HNO}_3$ process as it is a developing field. Since there are currently no benchmark catalysts with greater performance for researchers to compare, a broader objective should be proposed for future pathways. Consequently, it is calculated that takes into account both the current market price of HNO_3 and the desired catalytic performance of the materials. The developed materials are currently not competitive with traditional methods like Haber–Bosch process and Ostwald process. It is noted that the estimated cost of HNO_3 generation in the Haber–Bosch and Ostwald process is $890 \text{ € t-HNO}_3^{-1}$ for 20 € MW h^{-1} energy consumption. The current market price of HNO_3 is around $250\text{--}350 \text{ € t-HNO}_3^{-1}$. The relatively low cost of fossil–based feedstock, such as natural gas and coal, is a major reason for the relatively low market price of HNO_3 . [21, 75] It is important to develop effective catalysts with high efficiency, especially those that operate at low potential. In addition to discussing potential advances in N_2OR , we can focus on an intuitive assessment of catalysts.

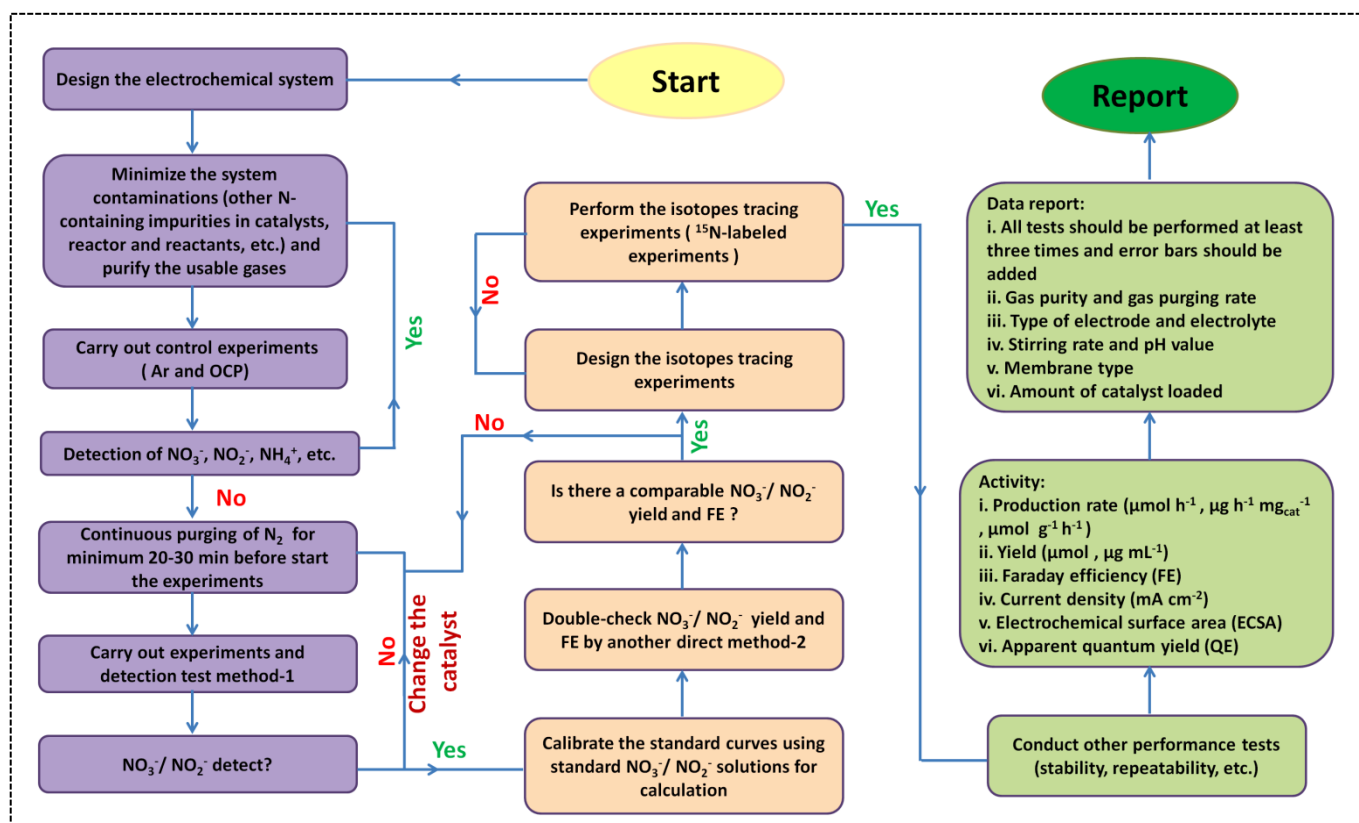


Figure 11: N_2OR synthesis protocol

9. Conclusion

An effective electrochemical N_2 to N_2OR conversion, provides a greener option than the conventional Ostwald process, enhances the ease of access and chemical storage of renewable energy, thereby paving the way for renewable energy and a sustainable future. Several benefits of N_2OR are highlighted in order to encourage promoting research on this field. By offering precise, exclusive and extensive evaluation indices, our research aims to promote the design and selection of electrocatalysts for N_2OR . In conclusion, it is advantageous to develop durable and environmentally friendly electrocatalysts for electrocatalytic N_2OR in ambient conditions. A roadmap for developing nitrate/nitric acid synthesis protocols is provided for better understanding. However, the catalysts that are

currently being researched and reported do not have a high yield rate and FE, a sufficient number of active sites, suitable adsorption kinetics, or sufficient stability. Along with logical design, thorough characterization, theoretical studies, and reliable nitrate/nitric acid detection, the real challenges of N₂OR will be investigated. For a new generation, electrochemical nitric acid production is a whole new avenue for research. The scientific community from all backgrounds must collaborate on this.

Acknowledgement: UKG also acknowledges Science & Technology and Biotechnology Department, Govt. of West Bengal for providing the financial support [199 (Sanc.)/ST/P/S&T/6c-12/2018]. A.A. would like to thank Science & Technology and Biotechnology Department, Govt. of West Bengal for providing JRF.

Notes: UKG, AA and SP have filed an Indian patent application (202131029797) regarding the electrochemical synthesis of nitric acid process under ambient conditions.

References:

1. J. N. Galloway, F. J. Dentener, D. G. Capone, E. W. Boyer, R. W. Howarth, S. P. Seitzinger, G. P. Asner, C. C. Cleveland, P. A. Green, E. A. Holland, D. M. Karl, A. F. Michaels, J. H. Porter, A. R. Townsend, C. J. Voron'smarty, *BioGeoCh*, 2004, **70**, 153–226.
2. D. Fowler, M. Coyle, U. Skiba, M. A. Sutton, J. N. Cape, S. Reis, L. J. Sheppard, A. Jenkins, B. Grizzetti, J. N. Galloway, P. Vitousek, A. Leach, A. F. Bouwman, K. Butterbach-Bahl, F. Dentener, D. Stevenson, M. Amann and M. Voss, *Philos. Trans. R. Soc. B Biol. Sci.*, 2013, **368**, 20130164–20130164.
3. R. D. Hill, R. G. Rinker, H. D. Wilson, *J. Atmos. Sci.* 1980, **37**, 179–192.

4. A. Masarwa, D. Didier, T. Zabrodski, M. Schinkel, L. Ackermann and I. Marek, *Nature*, 2014, **505**, 199–203.
5. Z. Zhang, K. Tanaka and J. Q. Yu, *Nature*, 2017, **543**, 538–542.
6. Erisman, *Glob. Chang. Biol.*, 2008, **14**, 2057–2063.
7. K. Arashiba, Y. Miyake and Y. Nishibayashi, *Nat. Chem.*, 2011, **3**, 120–125.
8. D. E. Canfield, A. N. Glazer and P. G. Falkowski, *Science (80-.)*, 2010, **330**, 192–196.
9. S. V, *Global Biogeochem. Cycles*, 1999, **13**, 647–662.
10. P. G. Levi and J. M. Cullen, *Environ. Sci. Technol.*, 2018, **52**, 1725–1734.
11. Van der Hoeven, M.; Kobayashi, Y.; Diercks, R. Technology roadmap: Energy and GHG reductions in the chemical industry via catalytic processes. International Energy Agency, 2013.
12. P. Vrrousek, *Ecology*, 1994, **75**, 1861–1876.
13. F. Haber, R. Leiser, Method and apparatus for testing gases. U.S. Patent 1,269,599, June 18, 1918.
14. Technavio. Nitric Acid Market by Application and Geography - Forecast and Analysis 2020–2024. Dec 2020; <https://www.technavio.com/report/nitric-acid-market-industry-analysis>.
15. Fior Markets. Nitric acid Market by Type (Strong, Fuming), Application (Nitrobenzene, Adipic Acid, Ammonium Nitrate, Toluene Diisocyanate), End-use Industry (Explosives, Agrochemicals, Electronics, Automotive, Others), Region, Global Industry Analysis, Market Size, Share, Growth, Trends, and Forecast 2021 to 2028. Report ID: 419494, June 2021; <https://www.fiormarkets.com/report/nitric-acid-market-by-type-strong-fuming-application-419494.html>.
16. Grand View Research. Nitric Acid Market Size, Share & Trends Analysis Report By

Application (Fertilizers, Adipic Acid, Nitrobenzene, Toluene Di-isocyanate, Nitrochlorobenzene), By Region, And Segment Forecasts, 2020 - 2027. Report ID: 978-1-68038-441-3, March 2020; <https://www.grandviewresearch.com/industry-analysis/nitric-acid-market>.

17. M. Kitano, Y. Inoue, Y. Yamazaki, F. Hayashi, S. Kanbara, S. Matsuishi, T. Yokoyama, S. W. Kim, M. Hara and H. Hosono, *Nat. Chem.*, 2012, **4**, 934–940.
18. Y. Wang, Y. Yu, R. Jia, C. Zhang and B. Zhang, *Natl. Sci. Rev.*, 2019, **6**, 730–738.
19. Y. Liu, M. Cheng, Z. He, B. Gu, C. Xiao, T. Zhou, Z. Guo, J. Liu, H. He, B. Ye, B. Pan and Y. Xie, *Angew. Chemie - Int. Ed.*, 2019, **58**, 731–735.
20. A. J. Medford and M. C. Hatzell, *ACS Catal.*, 2017, **7**, 2624–2643.
21. Y. Wang, T. Li, Y. Yu and B. Zhang, *Angew. Chem. Int. Ed.* 2022, **61**, e202115409.
22. T. Li, S. Han, C. Wang, Y. Huang, Y. Wang, Y. Yu and B. Zhang, *ACS Catal.*, 2021, **11**, 14032–14037.
23. L. Zhang, M. Cong, X. Ding, Y. Jin, F. Xu, Y. Wang, L. Chen and L. Zhang, *Angew. Chemie - Int. Ed.*, 2020, **59**, 10888–10893.
24. C. Dai, Y. Sun, G. Chen, A. C. Fisher and Z. J. Xu, *Angew. Chemie - Int. Ed.*, 2020, **59**, 9418–9422.
25. S. Han, C. Wang, Y. Wang, Y. Yu and B. Zhang, *Angew. Chemie - Int. Ed.*, 2021, **60**, 4474–4478.
26. Y. Zhang, F. Du, R. Wang, X. Ling, X. Wang, Q. Shen, Y. Xiong, T. Li, Y. Zhou and Z. Zou, *J. Mater. Chem. A*, 2021, **9**, 17442–17450.
27. W. Fang, C. Du, M. Kuang, M. Chen, W. Huang, H. Ren, J. Xu, A. Feldhoff and Q. Yan, *Chem. Commun.*, 2020, **56**, 5779–5782.
28. M. Kuang, Y. Wang, W. Fang, H. Tan, M. Chen, J. Yao, C. Liu, J. Xu, K. Zhou and Q. Yan, *Adv. Mater.*, 2020, **32**, 1–7.

29. J. Lan, M. Luo, J. Han, M. Peng, H. Duan and Y. Tan, *Small*, 2021, **17**, 1–7.
30. Y. Guo, S. Zhang, R. Zhang, D. Wang, D. Zhu, X. Wang, D. Xiao, N. Li, Y. Zhao, Z. Huang, W. Xu, S. Chen, L. Song, J. Fan, Q. Chen and C. Zhi, *ACS Nano*, 2022, **16**, 655–663.
31. R. Johnson, III NIST Computational Chemistry Comparison and Benchmark Database; NIST Standard Reference Database No. 101, Release 15b; NIST: Gaithersburg, MD, 2011.
32. Remsen, I.; Renoup, H. (1906). "The Oxidation of Atmospheric Nitrogen with Reference to the Manufacture of Nitrates and Nitric Acid" (PDF). *American Chemical Journal*. 35: 358–367. Retrieved 1 February 2019.
33. Karl Fisher; William E. Newton (2002). G. J. Leigh (ed.). *Nitrogen fixation at the millennium*. Elsevier. pp. 2–3. ISBN 0-444-50965-8.
34. Webb, H. W. (1923). *Absorption of Nitrous Gases*. Edward Arnold & Co. p. 20.
35. Alan V. Jones; M. Clemmet; A. Higton; E. Golding (1999). Alan V. Jones (ed.). *Access to chemistry*. Royal Society of Chemistry. p. 250. ISBN 0-85404-564-3.
36. J. G. Chen, R. M. Crooks, L. C. Seefeldt, K. L. Bren, R. Morris Bullock, M. Y. Darensbourg, P. L. Holland, B. Hoffman, M. J. Janik, A. K. Jones, M. G. Kanatzidis, P. King, K. M. Lancaster, S. V. Lymar, P. Pfromm, W. F. Schneider and R. R. Schrock, *Science*, 2018, **360**, eaar6611.
37. G. F. Han, F. Li, Z. W. Chen, C. Coppex, S. J. Kim, H. J. Noh, Z. Fu, Y. Lu, C. V. Singh, S. Siahrostami, Q. Jiang and J. B. Baek, *Nat. Nanotechnol.*, 2021, **16**, 325–330.
38. C. Tang and S. Z. Qiao, *Chem. Soc. Rev.*, 2019, **48**, 3166–3180.
39. J. Chen, C. Chen, M. Qin, B. Li, B. Lin, Q. Mao, H. Yang, B. Liu and Y. Wang, *Nat Commun*, 2022, **13**, 5382.

40. M. Jin, X. Zhang, S. Niu, Q. Wang, R. Huang, R. Ling, J. Huang, R. Shi, A. Amini and C. Cheng, *ACS Nano*, 2022, **16**, 11577–11597.
41. S. Murmu, S. Paul, S. Kapse, R. Thapa, S. Chattopadhyay, A. N., S. N. Jha, D. Bhattacharyya and U. K. Ghorai, *J. Mater. Chem. A*, 2021, **9**, 14477–14484.
42. U. K. Ghorai, S. Paul, B. Ghorai, A. Adalder, S. Kapse, R. Thapa, A. Nagendra and A. Gain, *ACS Nano*, 2021, **15**, 5230–5239.
43. J. Lan, M. Luo, J. Han, M. Peng, H. Duan and Y. Tan, *Small*, 2021, **17**, 1–7.
44. X. Cui, C. Tang and Q. Zhang, *Adv. Energy Mater.*, 2018, **8**, 1–25.
45. S. Wang, F. Ichihara, H. Pang, H. Chen and J. Ye, *Adv. Funct. Mater.*, 2018, **28**, 1–26.
46. M. Kitano, Y. Inoue, Y. Yamazaki, F. Hayashi, S. Kanbara, S. Matsuishi, T. Yokoyama, S. W. Kim, M. Hara and H. Hosono, *Nat. Chem.*, 2012, **4**, 934–940.
47. C. G. Zhan, J. A. Nichols and D. A. Dixon, *J. Phys. Chem. A*, 2003, **107**, 4184–4195
48. T. Li, S. Han, C. Cheng, Y. Wang, X. Du, Y. Yu and B. Zhang, *Angew. Chemie - Int. Ed.*, 2022, **61**, e202204541.
49. S. Zhang, T. Shi, K. Li, Q. Sun, Y. Lin, L. R. Zheng, G. Wang, Y. Zhang, H. Yin and H. Zhang, *J. Phys. Chem. C*, 2022, **126**, 965–973.
50. A. Adalder, S. Paul, B. Ghorai, S. Kapse, R. Thapa, A. N. and U. K. Ghorai, *ChemRxiv*, 2022, 1–18.
51. X. Zhang, E. A. Davidson, D. L. Mauzerall, T. D. Searchinger, P. Dumas and Y. Shen, *Nature*, 2015, **528**, 51–59.
52. M. Légaré, G. Bélanger-Chabot, R. Dewhurst, E. Welz, I. Krummenacher, B. Engels and H. Braunschweig, *Science (80)*, 2018, **359**, 896–900.
53. C. Liu, Q. Li, C. Wu, J. Zhang, Y. Jin, D. R. Macfarlane and C. Sun, *J. Am. Chem. Soc.*, 2019, **141**, 2884–2888.

54. Y. Wan, J. Xu and R. Lv, *Mater. Today*, 2019, **27**, 69–90.
55. H. Liu, L. Wei, F. Liu, Z. Pei, J. Shi, Z. J. Wang, D. He and Y. Chen, *ACS Catal.*, 2019, 5245–5267.
56. J. Huang, Y. Sun, Y. Zhang, G. Zou, C. Yan, S. Cong, T. Lei, X. Dai, J. Guo, R. Lu, Y. Li and J. Xiong, *Adv. Mater.*, 2018, **30**, 1–9.
57. R. Pablo-Pedro, M. A. Magaña-Fuentes, M. Videa, J. Kong, M. Li, J. L. Mendoza-Cortes and T. Van Voorhis, *Nano Lett.*, 2020, **20**, 6336–6343.
58. T. Kou, M. Chen, F. Wu, T. J. Smart, S. Wang, Y. Wu, Y. Zhang, S. Li, S. Lall, Z. Zhang, Y. S. Liu, J. Guo, G. Wang, Y. Ping and Y. Li, *Nat. Commun.*, 2020, **11**, 1–10.
59. C. Yan, G. Chen, X. Zhou, J. Sun and C. Lv, *Adv. Funct. Mater.*, 2016, **26**, 1428–1436.
60. D. N. McIlroy, S. D. Hwang, K. Yang, N. Remmes, P. A. Dowben, A. A. Ahmad, N. J. Ianno, J. Z. Li, J. Y. Lin and H. X. Jiang, *Appl. Phys. A Mater. Sci. Process.*, 1998, **67**, 335–342.
61. X. Yu, P. Han, Z. Wei, L. Huang, Z. Gu, S. Peng, J. Ma and G. Zheng, *Joule*, 2018, **2**, 1610–1622.
62. M. Anand, C. S. Abraham and J. K. Nørskov, *Chem. Sci.*, 2021, **12**, 6442–6448.
63. D. D. Wagman, W. H. Evans, V. B. Parker, R. H. Schumm, I. Halow, S. M. Bailey, K. Churney and R. L. Nuttall, *J. Phys. Chem. Ref. Data*, 1982, 111–518.
64. G. Kresse and J. Hafner, *Phys. Rev. B*, 1993, **47**, 558–561.
65. G. Kresse and J. Hafner, *Phys. Rev. B*, 1994, **49**, 14251–14269.
66. G. Kresse and J. Furthmüller, *Comput. Mater. Sci.*, 1996, **6**, 15–50.
67. G. Kresse and J. Furthmüller, *Phys. Rev. B - Condens. Matter Mater. Phys.*, 1996, **54**, 11169–11186.

68. B. Hammer, L. B. Hansen and J. K. Nørskov, *Phys. Rev. B - Condens. Matter Mater. Phys.*, 1999, **59**, 7413–7421.
69. J. Wellendorff, K. T. Lundgaard, A. Møgelhøj, V. Petzold, D. D. Landis, J. K. Nørskov, T. Bligaard and K. W. Jacobsen, *Phys. Rev. B - Condens. Matter Mater. Phys.*, 2012, **85**, 32–34.
70. H. K. Lee, C. S. L. Koh, Y. H. Lee, C. Liu, I. Y. Phang, X. Han, C. K. Tsung and X. Y. Ling, *Sci. Adv.*, 2018, **4**, 1–9.
71. L. Li, C. Tang, B. Xia, H. Jin, Y. Zheng and S. Z. Qiao, *ACS Catal.*, 2019, **9**, 2902–2908.
72. D. Yao, C. Tang, L. Li, B. Xia, A. Vasileff, H. Jin, Y. Zhang and S. Z. Qiao, *Adv. Energy Mater.*, 2020, **10**, 1–8.
73. Fontana MG. Corrosion engineering. McGraw-Hill Education, New York, 2005
ISBN: 9780198700722.
74. P. Atkins and J. De Paula, *Atkins' physical chemistry*. 8th ed 2006.
75. K. H. R. Rouwenhorst, F. Jardali, A. Bogaerts and L. Lefferts, *Energy Environ. Sci.*, 2021, **14**, 2520–2534.